Nanoscale

ROYAL SOCIETY OF CHEMISTRY

PAPER

View Article Online
View Journal | View Issue

Cite this: *Nanoscale*, 2025, **17**, 14727

Controlling the formation of fast-growing silver nanocubes in non-polar solvents†

Maximilian Joschko, [a,b] Moritz Schattmann,[a,b] Deniz Grollmusz[a,b] and Christina Graf *[a,b]

The key to the most efficient nanostructures is a deep understanding and control of all factors influencing the reaction mechanism. To realize the full potential of a synthesis of Ag nanocubes in a non-polar solvent mixture, the factors that determine the results are thoroughly investigated. In this hot-injection approach, an Ag precursor reacts with a Cl precursor to form AgCl and multiply twinned (MT) Ag nanoparticles. The AgCl is then reduced to single crystalline Ag nanoparticles while the MT nanoparticles are oxidized. As a result, the single crystals grow into nanocubes. Previously unidentified factors like the catalytic influence of Fe(III) ions and the *in situ* formation of HCl, which leads to an undefined chloride content, are revealed. A high reproducibility is achieved by controlling the amount of Fe(III) ions and adding a stable Cl source. Thoroughly investigating and combining the effects of chloride concentration with temperature and oxidative etching allows for adjusting the edge length of the nanocubes in the range of 40 to 100 nm and improving their uniformity. These findings lead to a robust protocol for producing non-polar silver nanocubes with sharp edges, low polydispersity, tunable size, and thus tunable optical properties in a short reaction time.

Received 2nd April 2025,
Accepted 21st May 2025

DOI: 10.1039/d5nr01350j

rsc.li/nanoscale

Introduction

The range of applications for silver today is broad and includes jewelry, currency, medicine, imaging, electronics, and pharmaceuticals.[1] However, at the nanoscale, silver unfolds the full potential of its antimicrobial and electrical properties and even shows new properties, such as localized surface plasmon resonance.[2] The nanoparticles can be used for electronic devices,[3–5] as sensors,[6–8] as antimicrobials,[9–11] in (photo) catalysis,[12–14] or surface-enhanced Raman spectroscopy (SERS).[15–17]

Some of the applications require special particle shapes in order to make optimum use of the properties of the silver nanoparticles. For example, electromagnetic hotspots, which increase SERS sensitivity, are strongly amplified at sharp edges of metallic nanoparticles.[18] Hence, particle shapes such as cubes, stars, pyramids, or prisms are advantageous. Other examples are particle shapes that have specific crystal surfaces and, therefore, enhance different catalytic activities. So, the {111} facet of silver increases oxygen reduction reactions or the reduction of methylene blue,[19,20] while the {100} facet enhances styrene oxidation and ethylene epoxidation.[21,22]

Since the {111} facets are thermodynamically more stable than the {100} facets, the nanoparticles preferably form multiply twinned (MT) structures that consist mainly or even entirely of {111} facets.[23,24] The synthesis of nanoparticles that have only {100} facets, *i.e.*, a nanocube, is therefore a major challenge. Such a nanocube can only grow from a single crystalline (SC) seed particle. Due to the cubic crystal structure of silver, this seed consists of 6 {100} and 8 {111} facets. If the {100} facets are sufficiently stabilized, the nanoparticle will grow only on the other facets and eventually take the shape of a cube.

The most popular method for achieving cubic growth of silver nanoparticles is the polyol synthesis. The first Ag nanocubes were obtained by this method in 2002 by the Xia group. They used $AgNO_3$ as Ag precursor, polyvinylpyrrolidone (PVP) as stabilizing and shape-directing agent, and ethylene glycol as solvent and reducing agent.[25] Over the next 20 years, the Xia group studied and optimized the synthesis by examining the influence of chloride and oxygen as MT oxidizing agents,[26] adding Fe^{II}/Fe^{III} as oxygen scavenger system to improve the sharpness of the nanocubes,[24] adding a hydrogen and sulfide

[a]*Hochschule Darmstadt – University of Applied Sciences, Fachbereich Chemie- und Biotechnologie, Stephanstr. 7, D-64295 Darmstadt, Germany.*
E-mail: christina.graf@h-da.de
[b]*EUt+ Institute of Nanomaterials & Nanotechnologies EUTINN, European University of Technology, European Union*

† Electronic supplementary information (ESI) available: Information on synthesis variations, particle purification, and characterization; additional SEM/TEM images; IR, XRD, and additional photographs. See DOI: **https://doi.org/10.1039/d5nr01350j**

source as oxidizing and reduction agents,[27–30] and studying the influence of other polyols,[31] different Ag precursors,[32] or additional stabilizers.[33] After the first successful synthesis, some protocols for seed-mediated and aqueous syntheses were also developed.[34–37] However, all of these protocols yield nanocubes that are stable in polar solvents.

If an application in a non-polar medium is desired, *e.g.*, catalysis in organic solvents or SERS of organic molecules, nanocubes synthesized in non-polar media are preferred. In addition, due to their long-chained organic ligands, such particles can be used in flexible plasmonic substrates or for self-assembly at interfaces.[38,39] While there are some studies on the synthesis of Ag nanoparticles in non-polar solvents,[40–42] reports on the synthesis of Ag nanocubes in non-polar organic solvents are rare. Two groups of authors use dichlorobenzene as a solvent.[43,44] Although the results look promising, the synthesis is time-consuming (48 h), and dichlorobenzene must be handled with care as it is a CMR substance. Another protocol was developed by Ma *et al.*, who used Fe(III) species as an etching component in the solvent isoamyl ether.[45] They were able to obtain small nanocubes (~13.5 nm) but with truncated corners. In a third approach, $AgNO_3$ and dimethyldistearylammonium chloride (DDAC) in an octyl ether/oleylamine mixture were used to initially obtain AgCl and Ag MT nanoparticles *via* the hot-injection method.[46,47] Subsequently, the AgCl nanoparticles transform into Ag SC nanoparticles, which grow into nanocubes at the expense of dissolving Ag MT nanoparticles. By this method, the authors Peng and Sun obtain uniform Ag nanocubes with a diameter of ~35 nm and sharp corners after 1 h reaction time. Unfortunately, the role and influence of the different chemicals involved and even the role of the experimental setup are only roughly understood. Thus, this synthesis is difficult to control and hardly reproducible.[43] However, as the Ag nanocubes in this synthesis grow quickly, are of high quality, and come from non-toxic chemicals, it is an excellent starting point for optimization.

The objective of this work is to identify the main factors affecting the reproducibility and the quality of Ag nanocubes synthesized in non-polar solvents and to develop strategies to control these factors. It will be demonstrated that iron ions are crucial as catalysts for the formation of the Ag nanocubes, which were probably previously introduced into the synthesis unnoticed using a metal thermometer. Decisive for the success of the synthesis and the quality of the resulting nanocubes is also the Cl : Ag ratio in the reaction mixture. The originally used DDAC decomposes upon heating and releases HCl, resulting in an uncontrolled varying Cl : Ag ratio. This issue can be circumvented by replacing the DDAC with oleylammonium chloride (OlAmoCl), which can be pre-synthesized, is temperature-stable, and is likely to be the final chloride component in the original synthesis. In this context, the role of the solvent, the influence of the Cl : Ag ratio, the oxidizing agent, and the dependence of the results on the temperature were examined in more detail. By conducting a comprehensive evaluation of all these factors, we have developed a new synthesis protocol that allows for the control of the edge length of the nanocubes in the range between 40 and 100 nm and ensures high reproducibility.

Experimental section

All experiments were conducted using standard glassware. Prior to the synthesis, each reaction vessel was cleaned with nitric acid (65%, Fisher Scientific) and subsequently rinsed with deionized (DI) water. An LTR3500 digital temperature controller (Juchheim Solingen) connected to a PT100 glass thermometer (Juchheim Solingen) was used for heating and temperature control. The sonication bath used for the redispersion of the nanoparticles was a Sonorex RK512H (860 W, 35 kHz; Bandelin). Unless otherwise indicated, all synthesis steps are performed under a constant argon flow (~1 L h^{-1}).

Materials

Silver nitrate (99.9999%), iron(III) chloride hexahydrate (≥99%), dibenzyl ether (≥98%, DBE), oleylamine (≥98% primary amine, OlAm), silver acetate (99.99%), and ammonium nitrate (≥99%) were obtained from Sigma Aldrich. Dimethyldistearylammonium chloride (DDAC) was ordered from fluorochem, hydrochloric acid (32%) from VWR, and 1-octadecene (90% tech., ODE), acetone (99+ %) and hexane (mixed isomers, 98+ %) from Thermo Scientific. All chemicals were used as received and without further purification.

Synthesis details

Synthesis of oleylammonium chloride (OlAmoCl). For the synthesis of the chloride precursor OlAmoCl, a modified procedure from Dutta *et al.* was used.[48] To receive a solution of 1 M OlAmoCl in oleylamine (OlAm), 61.08 mL OlAm was stirred in a 100 mL Schlenk flask under an argon atmosphere. After adding 6 mL of hydrochloric acid (32%), a white precipitate formed immediately. Subsequently, the mixture was heated to 120 °C and kept at this temperature under an argon flow for 2 h to remove most of the water. The remaining water was removed by applying a vacuum (0.05 mbar) at 60 °C for 1 h. The mixture solidified at ambient temperature and was stored as a stock solution at 8 °C in an argon atmosphere.

The chloride content was verified by Mikroanalytisches Labor Kolbe, Oberhausen, Germany, with ion chromatography with a Metrohm Model 930 Compact IC Flex Oven/SeS/PP/Deg after a combustion digestion in an AQF-2100H from Mitsubishi.

Standard synthesis. Two precursor solutions were prepared for the synthesis of Ag nanocubes.

The chloride precursor was prepared in a 50 mL three-neck round-bottom flask. 0.3 mL of a 3.7 mM (1 g L^{-1}) solution of $FeCl_3 \cdot 6H_2O$ in DBE was introduced as a catalyst and dispersed into a mixture of 20 mL of the solvent DBE and 2.07 mL of the reducing agent OlAm. In addition, 0.525 mL of a 1 M solution of OlAmoCl in solution was added. Under vigorous stirring (using a glass-covered stirring bar, 12 × 5 mm, VWR, 1300 rpm), the mixture was heated to 60 °C to liquefy the OlAmoCl.

Carefully, a vacuum was applied for 30 min (final pressure ~0.025 mbar). Subsequently, the system was purged with argon. This procedure was repeated twice (15 min each, final pressure ~0.02 mbar). The mixture was then heated up to 260 °C with a heating ramp of 10 K min^{-1} and kept at this temperature for 5 min until the temperature was stable.

Simultaneously, the silver precursor was prepared by dissolving $AgNO_3$ in OlAm to receive a 34.23 g L^{-1} (31.73 M) solution. The solution was heated to 50 °C, and a vacuum was carefully applied for 30 min (final pressure 0.025 mbar). It should be noted that $AgNO_3$ dissolves quite slowly in OlAm. The dissolution happens faster at 50 °C and when a weak vacuum (800–900 mbar) is applied. A vacuum was applied a second and a third time for 15 min each (final pressure ~0.02 mbar). However, the Ag precursor should not be prepared too far in advance, as the precursor will continue to react. This is indicated by a color change from pale yellow to a deeper yellow.

When both precursors had reached the desired temperature, the argon flow was stopped, and the Ag precursor was swiftly injected into the hot chloride precursor. A 3 mL disposable syringe (Romed) connected to a stainless-steel cannula (2.0 × 200 mm, neoLab) was filled to the 2.6 mL mark to inject 2.97 mL (2.6 mL syringe volume + 0.37 mL cannula volume) of the Ag precursor. After a 1 h reaction, the mixture was cooled to 200 °C with compressed air and then to 70 °C with an ice bath.

Optimized synthesis. The optimized synthesis results in fewer MT nanoparticles than the standard synthesis, but the lower size limit is slightly larger.

In principle, the optimized synthesis is performed in the same way as the standard synthesis. The difference is that a larger amount of the 1 M OlAmoCl in OlAm solution is used (0.545–0.57 mL) and that the reaction temperature is increased to 290 °C.

Synthesis variations, particle purification, and characterization

The different variations of the synthesis that were used in the presented studies, the particle purification procedure, and the section about the characterization methods can be found in the ESI.†

Results and discussion

The aim of the present research was to develop a controlled and practicable synthesis of silver nanocubes in a non-polar solvent mixture. Ideally, the reaction time should be as short as possible, the use of toxic chemicals should be avoided, the nanocubes should be of high quality, and the results should be highly reproducible. The studies conducted and discussed in this publication are based on the modified synthesis of silver nanocubes originally developed by Peng and Sun.[47] In brief, two precursor solutions were prepared. The first precursor contained 0.75 mmol dimethyldistearylammonium chloride (DDAC), 20 mL dioctyl ether (DOE), and 2.6 mL oleylamine (OlAm). After the dissolution of the DDAC at 60 °C, the solution was heated to 260 °C. At this temperature, the second precursor, containing 0.6 mmol $AgNO_3$ in 2.97 mL OlAm, was swiftly injected. The reaction was continued for 1 h. All reaction steps were performed under a constant argon flow.

During the studies of the current work, DOE was replaced by dibenzyl ether (DBE) as the results seemed to be more reproducible. However, it likely makes no difference whether DOE or DBE is used.

Catalytic influence of iron

The first attempts to establish the synthesis by Peng and Sun yielded spherical nanoparticles within a size (diameter) range of 10–30 nm instead of nanocubes with an edge length of 35–40 nm and a narrow size distribution, as reported by the authors. Particles of one of the first syntheses are displayed in a scanning electron microscopy (SEM) micrograph in Fig. 1(a).

After several parameters have been varied (temperature, amount of DDAC, duration, solvent), the nanocubes shown in Fig. 1(b) were finally obtained. However, the only change that was made compared to the synthesis from Fig. 1(a), was to replace the previously used glass thermometer with one made from steel. To verify that the nanocubes were not simply the result of an unidentified influence, a second experiment was conducted. The thermometer material was changed back to glass, and a piece of a steel capillary of comparable length and diameter to the immersed part of the thermometer was placed in the reaction flask. As can be seen from Fig. 1(c), the nanocubes were of the same quality as the ones received from the synthesis with the steel thermometer. Apparently, the steel had a significant influence on the formation mechanism of the silver nanocubes.

As metals are known for their potential catalytic properties and iron is the main component of the V4A stainless steel used in the thermometer, a small amount of $FeCl_3 \cdot 6H_2O$ (43 μM) was introduced into a third experiment with a glass thermometer and no steel components. The high quality of the nanocubes obtained, as shown in Fig. 1(d), strongly indicates that Fe ions catalyze the formation of silver nanocubes in this synthesis approach.

Formation of the chloride precursor

Not long after, another problem with the synthesis occurred. A silver mirror appeared irregularly on the walls of the reaction flask directly after the injection. Whenever the silver mirror appeared, the resulting nanoparticles were spherical, smaller, and more polydisperse than the expected nanocubes. A photograph of a typical silver mirror, as well as the resulting nanoparticles, can be found in Fig. S1 in the ESI.†

Simultaneously with the synthesis (with or without a silver mirror) and even before the injection of the $AgNO_3$ solution, it was observed that a reflux product was forming in the condenser, which led to a bumping effect when it dripped into the reaction solution. This product must, therefore, have a boiling point below the reaction temperature and thus be a component that is formed *in situ*. All initial reaction components have a boiling temperature above the reaction temperature.

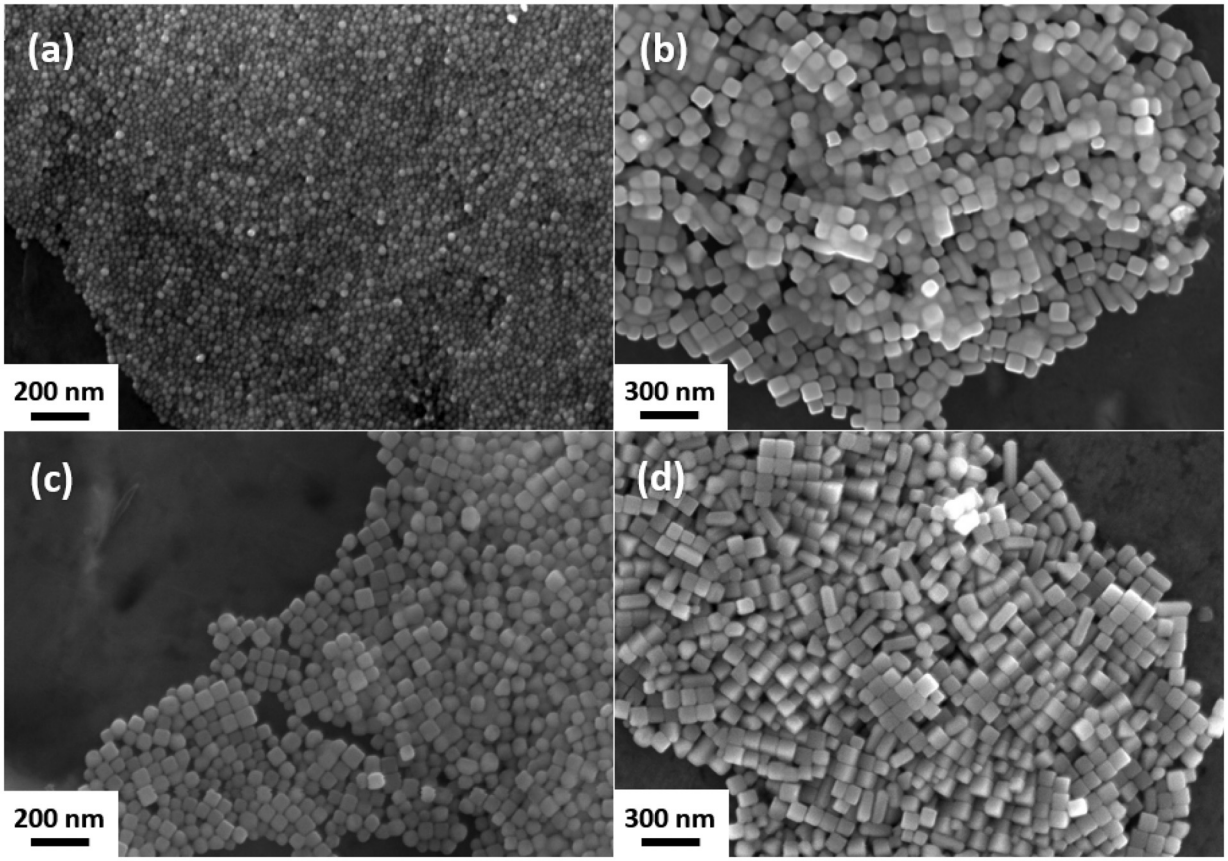

Fig. 1 SEM images of Ag nanoparticles synthesized with and without exposure to different metal surfaces: (a) no metals used (glass thermometer), (b) steel thermometer used, (c) V4A steel capillary used with a glass thermometer, and (d) $FeCl_3{\cdot}6H_2O$ powder used with a glass thermometer.

The reflux product was captured and analyzed with IR spectroscopy. The comparison of the IR spectrum with the standard reference from the NIST webbook[49] (see Fig. S2(a), ESI†) shows that the unknown substance is water without any organic compounds. In an additional test for halogenides (Fig. S2(b)–(d), ESI†), the reflux water was added to a 1 M $AgNO_3$ solution.[50] The immediately precipitating white substance was then dissolved in a 25% ammonia solution. This suggests that chloride is dissolved in the reflux water. The same results were obtained without iron ions present in the synthesis. Since no organic compounds could be detected in the reflux water and no inorganic ions were present in the experiment, HCl is the most likely substance in the reflux water.

The above-described studies suggest that water and HCl are formed during the heat-up of the chloride precursor. This theory is supported by the work of Frederick and Bell, who investigated the cleavage of DBE in the presence of zinc halides.[51] In the presence of $ZnCl_2$, two of the cleavage byproducts are water and HCl. Given the presence of both DBE and DDAC (which contains chlorine) in the current synthesis and the fact that DDAC begins to decompose at ~220 °C,[52] a possible mechanism could involve the reaction of DBE and DDAC at elevated temperatures, which produces water and HCl, along with other products. However, HCl is a gaseous product and is likely to outgas during synthesis, especially at higher temperatures. As chloride is necessary for the formation of the silver nanocubes, it is reasonable to assume that the HCl continues to react and, thus, remains in the reaction mixture. The most likely reaction partner is OlAm, which would result in the formation of the temperature-stable compound OlAmoCl.[53,54]

Assuming that HCl is formed during the heating of the synthesis, the rate of constant inert gas (argon) flow would affect the final chloride content at injection. To verify this hypothesis, the experiments were repeated in a static argon atmosphere instead of a constant argon flow. More reproducible results regarding the cubic shape of the received nanoparticles were obtained, and there was no longer any random occurrence of silver mirrors. Although this strengthens the assumption that HCl is formed, further evidence was needed that DBE and DDAC are necessary for the formation of HCl and that HCl and OlAm react to form OlAmoCl.

Thus, four experiments were designed. At first, the standard experiment with DBE and DDAC (0.64 mmol) was compared with an experiment in which DBE was replaced by 1-octadecene (ODE). Subsequently, both experiments were repeated, but DDAC was replaced by pre-synthesized OlAmoCl (0.52 mmol). In the OlAmoCl experiments, a lower concen-

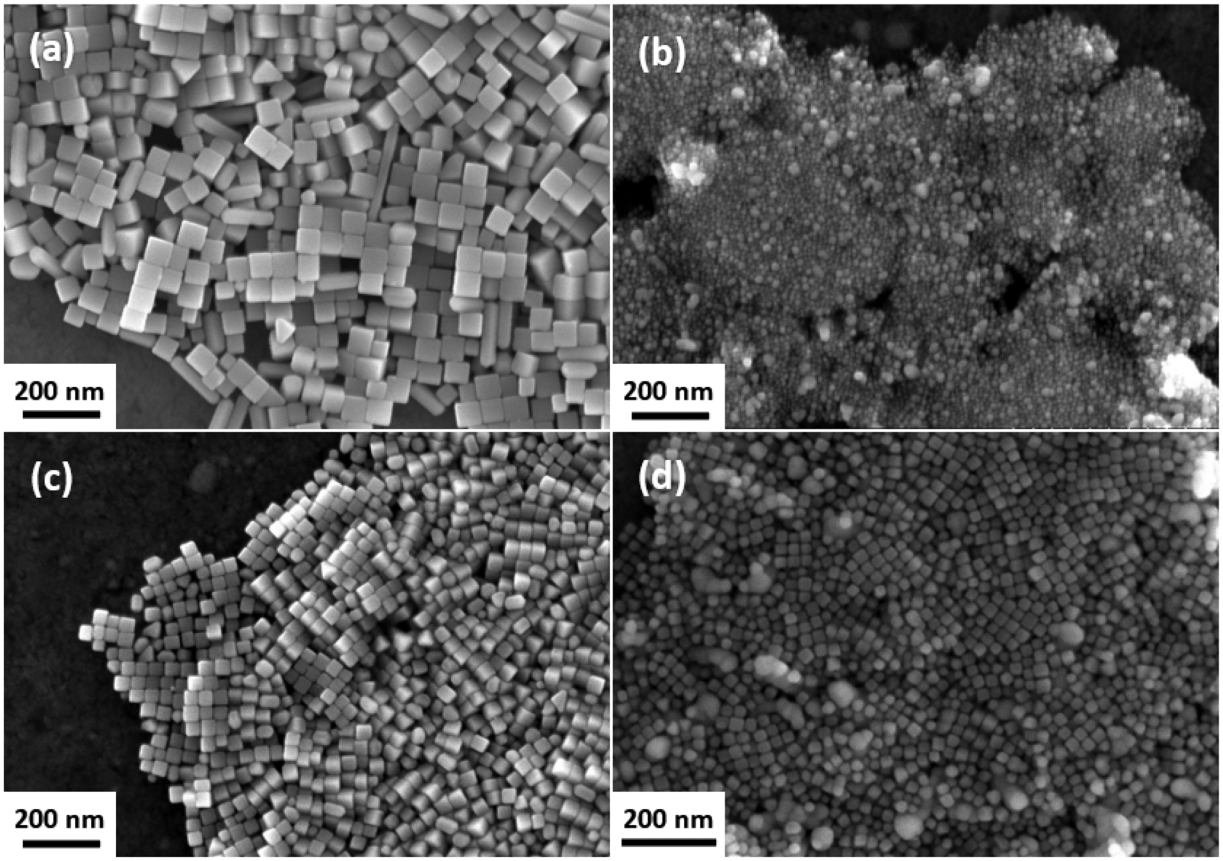

Fig. 2 SEM images of the silver nanocubes prepared in the experiments to investigate the influence of the solvent on the formation of nanocubes: synthesis with DDAC as chloride source and (a) DBE or (b) ODE as solvent and synthesis with OlAmoCl as chloride source and (c) DBE or (d) ODE as solvent.

tration of the chloride source was used as it was assumed that some of the formed HCl in the DDAC experiments would still outgas. SEM images of the resulting particles are shown in Fig. 2.

The following conclusions can be drawn from these results:

1. A comparison of the results for DBE + DDAC with those for ODE + DDAC reveals that the experiment with ODE did not yield any nanocubes but smaller, irregular nanoparticles with some bigger lumps in between. This is a strong indication that DBE is a crucial component in the reaction.

2. The results of both the DBE + DDAC and DBE + OlAmoCl experiments yielded high-quality nanocubes. However, the edge length of the nanocubes is different (~100 nm and ~65 nm, respectively). Hence, it can be concluded that OlAmoCl is either another usable chloride source or the final effective chloride component in the DDAC experiments and that the chloride content may influence the size of the nanocubes. The latter will be discussed in the next section.

3. Comparing DBE + OlAmoCl and ODE + OlAmoCl, the quality of the nanocubes is higher when DBE was used, *i.e.*, the cubes have sharper corners, are more uniform, and no larger undefined lumps are present in the sample. Although nanocubes could be obtained with ODE as solvent, it seems that DBE has some impact on the final nanocubes. This is because the ether group makes the reaction medium at least slightly polar, enhancing ion mobility and transfer.[44]

4. A comparative analysis of the ODE + DDAC and ODE + OlAmoCl syntheses indicates that OlAmoCl functions as the final chloride component while DDAC does not. Since DDAC is not temperature-stable and does not form HCl and, subsequently, OlAmoCl in ODE, a large proportion of chloride is likely lost in the form of volatile chloro-organic compounds.[52]

To summarize this section, DBE (or rather an ether-based solvent, as DOE also works[47]) is a necessary component to produce Ag nanocubes when DDAC is used as the chloride source. DDAC cannot act as the final chloride component for the formation of AgCl due to its thermal instability and must react with DBE to form, among other products, HCl, which subsequently reacts with OlAm to OlAmoCl. In an inert solvent, DDAC likely decomposes into volatile chloro-organic compounds that outgas from the reaction mixture. When OlAmoCl is directly used as the chloride source, the synthesis results in nanocubes even in an inert solvent such as ODE, although the presence of DBE improves the quality of the nanocubes. Another advantage of directly using OlAmoCl is

that the reproducibility of the reaction is significantly improved.

Influence of the Cl : Ag ratio

Based on the reaction mechanism published by Peng *et al.*, it was assumed that particle nucleation and growth during this synthesis starts with the immediate formation of AgCl. Only a few moments later, Ag^+ is reduced by OlAm to form MT Ag nanoparticles. After ~1 min, Ag nuclei are formed on the AgCl particles, which subsequently convert into SC Ag nanoparticles. When all AgCl particles are converted, the SC Ag nanoparticles grow at the expense of the MT Ag nanoparticles.[46]

The results from the previous section indicate that the chloride content has a strong influence on the resulting final particles. Therefore, systematic studies with varying chloride contents were performed. To ensure that the chloride content at the moment of the injection of the $AgNO_3$ solution is the same as the chloride content that was initially added, OlAmoCl was used instead of DDAC in all following syntheses.

Three properties of the final samples were characterized and plotted against the Cl : Ag ratio: the size (edge length) of the nanocubes, the percentage of twins (MT nanoparticles) in relation to the total amount of Ag nanoparticles present in the sample, and the amount of AgCl relative to the total amount of Ag. The plots are shown in Fig. 3, along with four SEM images of four exemplary samples to give a visual impression of the chloride influence. Below is an explanation of how to distinguish MT and SC nanoparticles in the electron microscope.

Starting with low amounts of OlAmoCl, no AgCl could be found, and the nanoparticles had a size of about 20 nm. It also seems that this size marks the lower limit of the nanoparticle size range of this synthesis approach. Nevertheless, likely, the size will slowly decrease with a further decreasing Cl : Ag ratio. However, the nanoparticles appear to be little to no cubic at all (Fig. 3(b)). This is because the sample consists mainly of MT nanoparticles, which cannot grow into nanocubes. Based on the theory by Peng *et al.*, the amount of chloride is not sufficient to form initial AgCl, which subsequently is converted into SC Ag and etches the majority of the MT nanoparticles. Hence, the oxidation of the MT nanoparticles occurs much slower than the reduction of the Ag^+ ions, which leads to the growth of the MT nanoparticles. It is suggested that the SC Ag nanoparticles start growing on top of the AgCl at first, as AgCl can act as heterogeneous nucleation site for Ag nanoparticles.[55,56]

When the Cl : Ag ratio exceeds ~0.75, the size of the silver nanocubes starts to increase rapidly while the percentage of MT nanoparticles starts to decrease rapidly. Samples of high quality, *i.e.*, nanocubes with not more than slightly truncated corners, a polydispersity <10%, no AgCl present, and a majority of nanocubes instead of MT nanoparticles in the sample, are obtained within a range of Cl : Ag = ~0.84–0.88. Within this range, the edge length of the nanocubes is tunable from ~40–100 nm. Fig. 3(c) shows an SEM image of the sample prepared with a Cl : Ag ratio of 0.87. The sudden change in size and crystalline structure of the nanoparticles by only a slight variation of the Cl : Ag ratio can be explained by a competitive reaction between the reduction of Ag^+ by OlAm and the chloride-supported oxidation of Ag^0. As long as the Cl : Ag ratio is lower than a certain threshold, the reduction is too fast to lead to the formation of stable AgCl particles, which can then transform into SC Ag nanoparticles. The injected Ag^+ species are directly reduced, leading to the growth of the (MT) nanoparticles. However, as soon as enough chloride is present, stable AgCl particles can form and transform into SC Ag nanoparticles.

When the Cl : Ag ratio is increased further up to a ratio of 0.95 (see Fig. 3(d)), the edge length of the nanocubes approaches an upper limit of around 120–130 nm, and almost no more MT nanoparticles are found. However, the polydispersity of the samples increases drastically, and AgCl is found after 1 h reaction time. At this point, the oxidation of the silver nanoparticles occurs faster than the reduction. As a result, the less stable MT Ag nanoparticles are almost entirely etched, and the nucleation of the more stable SC Ag nanoparticles from the AgCl is slowed down so that the nanocubes grow larger and polydisperse, and the AgCl cannot be completely reduced anymore. However, the nanocubes have sharp edges and corners, which indicates that either the SC Ag nanoparticles are stable enough not to be etched or that more unstable silver species (*e.g.*, new Ag nuclei formed from the AgCl) are oxidized instead.

Increasing the Cl : Ag ratio even further leads to an increased formation of AgCl. The particle size and polydispersity will not change further until the Cl : Ag ratio is sufficiently high that there is not enough AgCl reduced for the SC Ag nanoparticles to grow into a cube, and, eventually, only AgCl is present after 1 h reaction time. A SEM image with mainly AgCl is shown in Fig. 3(e). The image shows Ag nanocubes with an edge length of ~120 nm between spherical particles with a diameter of up to 2 μm, which decompose in contrast to Ag nanoparticles in the electron beam. It is well-known that AgCl nano- and microparticles rapidly decompose under the electron beam.[57] Hence, this is a strong indication that these particles are AgCl.

An analysis with X-ray diffraction (XRD) (Fig. S3, ESI†) supports the SEM and EDX results. At a low Cl : Ag ratio, the diffractogram matches the reference pattern of bulk silver (COD 9008459) well. As the Cl : Ag ratio increases, the intensity of the (111) diffraction peak decreases while the intensity of the (200) diffraction peak increases. This is due to the fact that more Ag nanocubes are formed, which ideally would only consist of {100} planes. With an increasing Cl : Ag ratio, the first AgCl diffraction peaks (reference pattern: COD 9011666) start to appear until, eventually, the sample consists entirely of AgCl. This finding also strongly suggests that the large, rapidly decomposing particles in the SEM images (see Fig. 3(e)) are AgCl.

As already indicated in Fig. 2(c) and (d), at medium Cl : Ag ratios, short nanorods start to appear, which increase in length as the ratio increases. Nanorods are obtained when MT

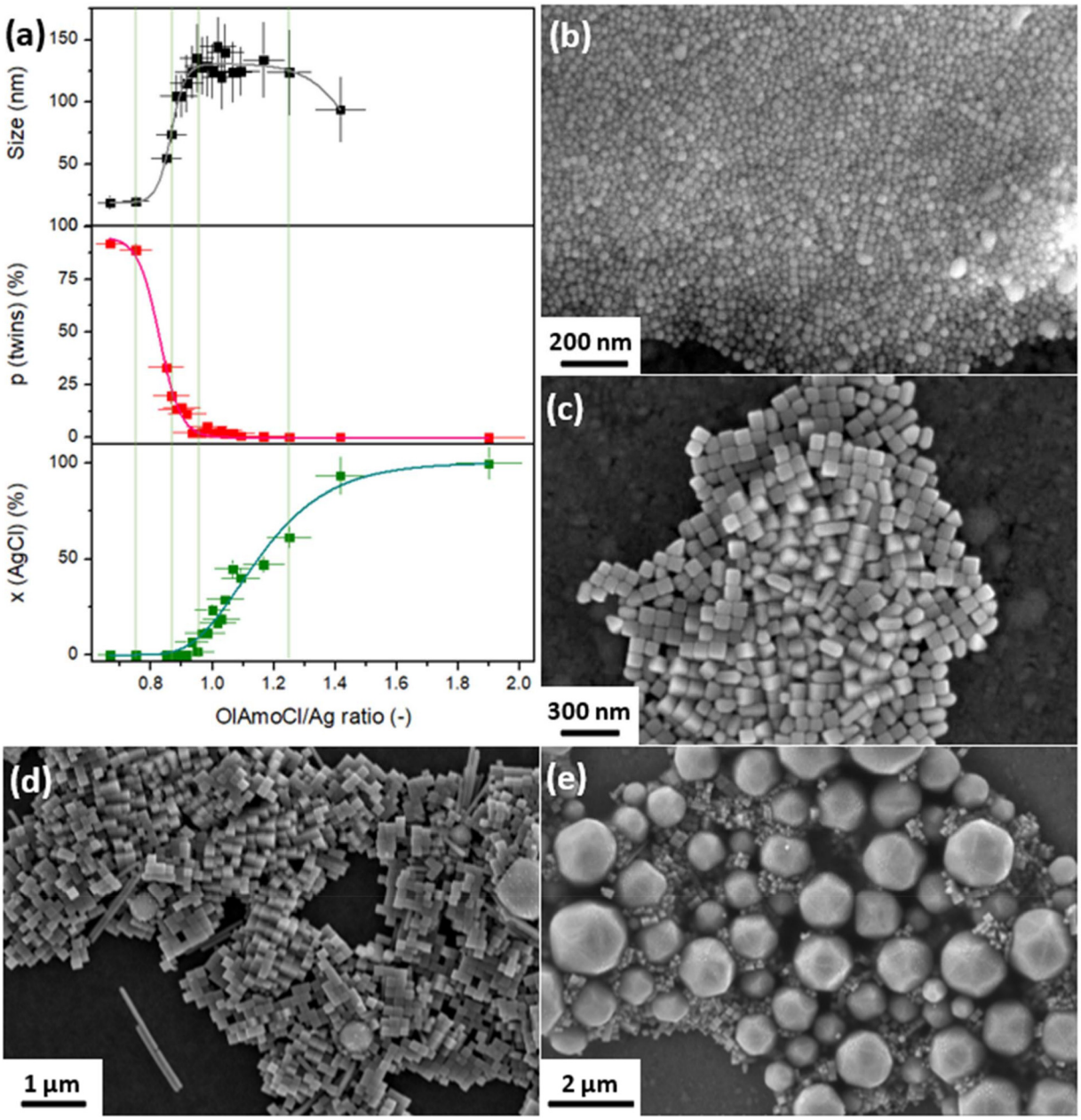

Fig. 3 (a) Influence of the Cl : Ag ratio on the edge length of the nanoparticles (top), on the occurrence of twinned nanoparticles (p = percentage of MT crystals in relation to the total amount of Ag nanoparticles) (middle), and the mass proportion of AgCl relative to Ag (bottom) in the final product. The green vertical lines mark the Cl : Ag ratios used in the synthesis of the particles shown in the exemplarily SEM images are (b) 0.75, (c) 0.85, (d) 0.93, and (e) 1.25.

Ag nanoparticles grow along one axis.[58] They are the most easily recognizable MT nanoparticles. However, even smaller, spherical MT nanoparticles can also be identified by TEM and even SEM images. Fig. S4 (ESI†) shows a TEM and two SEM images, giving a more detailed overview of a sample with smaller nanoparticles, a sample with medium-sized nanoparticles, and a sample with larger nanoparticles, respectively. In TEM (Fig. S4(a), ESI†), SC Ag nanoparticles exhibit a uniform contrast, while the MT nanoparticles show a blotchy contrast due to the different crystal facets. They also differ in shape from the SC nanoparticles so that both particle species can be distinguished in the SEM. This approach was verified by evaluating SEM and TEM images of the same samples, which led to the same result. This finding is important since the nanoparticles >50 nm are getting too thick to recognize the differences in contrast in TEM. Fig. S4(b) (ESI†) shows SEM images in which the MT nanoparticles are highlighted. In Fig. S4(c) (ESI†) one can see the rounded tip structure of the

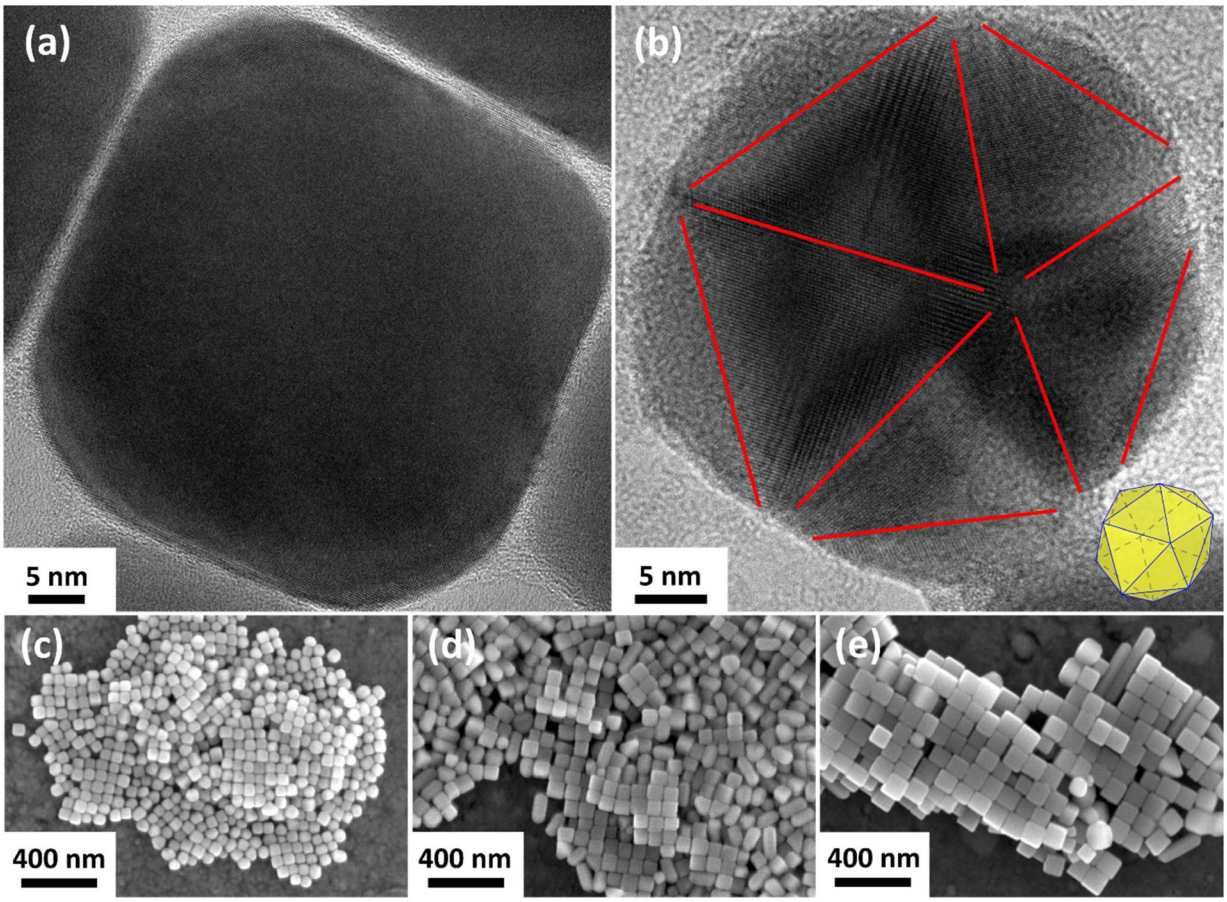

Fig. 4 Structural details of nanoparticles from different silver nanocube syntheses: HRTEM images of (a) an SC nanocube with an edge length of 45 nm in which a different lattice orientation can be recognized at the corners due to a slight truncation and (b) an MT nanoparticle (icosahedron) from the same sample. The red lines mark the twin boundaries, and a schematic of the nanoparticle is shown as an inset in the lower right corner. Figures (c)–(e) show SEM images of nanocubes with different edge lengths synthesized with 0.60 mmol Ag and (c) 0.51 mmol, (d) 0.52 mmol, and (e) 0.525 mmol OlAmoCl.

nanorods. This is typically observed because of the fivefold geometry of the tips. A detailed HRTEM analysis of an SC nanocube and an MT nanoparticle can be seen in Fig. 4(a) and (b), respectively. Since the nanocube has slightly truncated corners, a closer look at the corners reveals a different lattice structure than the otherwise uniform rest of the cube. When determining the twin boundaries of the MT nanoparticle in Fig. 4(b) (red marks), one can see its fivefold twinned structure and icosahedral shape. A schematic illustrating the position of the icosahedron is shown as an inset in the lower right corner of the image. Additionally, examples of size variations of the nanocubes are shown in Fig. 4(c)–(e) to emphasize the size adjustability of the nanocubes as a result of the findings presented in this section. While the nanocube in Fig. 4(a) is from a sample with an average nanocube edge length of 43 ± 5 nm (0.50 mmol chloride used with 0.60 mmol Ag), the nanocubes with a higher Cl : Ag ratio have an edge length of 55 ± 5 nm (0.51 mmol chloride, Fig. 4(c)), 74 ± 7 nm (0.52 mmol chloride), and 99 ± 9 nm (0.525 mmol chloride).

Oxidative etching and the role of oxygen

As has been shown so far, the OlAmoCl content has a significant influence on the oxidation of the MT nanoparticles. Although an increased oxidation rate was observed when the Cl : Ag ratio was increased, chloride itself is not oxidizing. This leads to the assumption that chloride likely supports the oxidation, but an oxidizing agent is needed in the reaction. Other authors mention oxygen,[35,43] Fe(III) species,[45] or nitrate[47] as oxidizing agents in silver nanocube syntheses. The most discussed one is oxygen. Some authors even actively enrich their syntheses with oxygen.[43] Thus far, the synthesis has been conducted in an oxygen-free environment, as the reaction mixture was degassed three times in a vacuum, and the reaction was carried out under an argon atmosphere. To study the influence of oxygen, defined quantities of oxygen were introduced into the synthesis by flushing the reaction vessel with Cargal, a mixture of argon with 2% oxygen, for defined periods after the reaction temperature was reached but before the injection of the $AgNO_3$ solution. To keep the solution at the temperature

plateau of 260 °C for an equivalent duration prior to the injection of the Ag precursor, an argon flow was applied for the remaining time after the shorter Cargal flushing periods. Two additional experiments were conducted, one using Cargal from the beginning of the heat-up procedure and one at ambient atmosphere. The results are shown in Fig. S5 (ESI†). Based on the results (Fig. S5(a), ESI†), the amount of oxygen in Cargal does not appear to affect the synthesis, even when it is used throughout the whole synthesis procedure. There is neither a change in size, polydispersity, nor the number of MT Ag nanoparticles. However, the color of the solution immediately prior to the injection of the Ag precursor changes from colorless when no Cargal was used (Fig. S5(b), ESI†) to a yellowish color. This color shift becomes more pronounced the longer Cargal is flushed over the synthesis mixture. While the reaction mixture retained a pale yellow when Cargal was used over the whole synthesis procedure (Fig. S5(c), ESI†), the color changed to a deep yellow when the synthesis was performed in ambient atmosphere (Fig. S5(d), ESI†). In this case, the resulting particles are significantly smaller (~30 nm instead of ~100 nm) than those prepared in argon or Cargal atmosphere and mainly spherical (Fig. S5(e), ESI†). These results suggest that oxygen does not affect the etching of the MT Ag nanoparticles. However, at significantly higher concentrations (*i.e.*, ambient conditions), O_2 could lead to the formation of iron oxide, which removes the iron ions from the catalytic cycle, or replace the chloride in the synthesis, which suppresses oxidative etching.

These considerations leave Fe(III) species, in this case $FeCl_3$, or nitrate as oxidizing agent. Since the amount of $FeCl_3$ is low in the synthesis (1.1 μmol) compared to 0.6 mmol Ag, it cannot be the main oxidizing agent. Although Fe(III) may be involved in the etching process, the reduced Fe(II) would need to be re-oxidized. Hence, the nitrate introduced into the reaction with the $AgNO_3$-oleylamine precursor solution most likely seems to be the main oxidation agent. Previous reports suggest it to be stable in the form of an amine-nitrate complex or a reaction product of nitrate and OlAm in high-boiling non-polar solvents.[59,60] To confirm this assumption, a synthesis without nitrate and a synthesis with an increased amount of nitrate were performed and compared to the standard synthesis. In Fig. 6, TEM images of the resulting Ag nanoparticles from a synthesis with silver acetate as precursor instead of $AgNO_3$ (Fig. 6(a)), the standard synthesis (Fig. 6(b)), and a synthesis with NH_4NO_3 added to the $AgNO_3$-OlAm precursor solution are compared. The images show that the less nitrate was present in the synthesis, the more MT nanoparticles were found. An evaluation of the quantity of MT nanoparticles yields an increase of 65% without nitrate and a decrease of 80% with additional nitrate compared to the standard synthesis, which proves the role of nitrate as the oxidizing agent.

Influence of temperature

The last parameter tested was the influence of the reaction temperature. The synthesis was performed at reaction temperatures from 220–280 °C, and three particle/synthesis characteristics were evaluated: As in the chloride studies, the particles were analyzed regarding their size and polydispersity as well as the percentage of MT nanoparticles. The fourth property examined was the duration of the color change of the reaction mixture, which occurs immediately following the injection of the Ag-OlAm precursor. The solution turns from a milky yellowish-white to orange and finally greenish-gray, indicating the progress of the reaction. The colors result from different particle species at different reaction stages. Almost instantly after injection, AgCl, which appears white, and small Ag MT nanoparticles, which are known for their yellowish color, have formed. As the AgCl is reduced and smaller silver species grow, the yellow color becomes more intense and darker, eventually appearing orange. When the SC Ag nanoparticles start to morph into a cubic shape and grow further, plasmon resonances and especially scattering cause the solution to appear greenish-gray in color. The results of the temperature studies are summarized in Fig. 5, and the corresponding SEM images are shown in Fig. S6 in the ESI.†

The duration of the initial color change decreases steadily with increasing temperature, which indicates that the reaction is progressing faster. This is expected as the reaction kinetics are enhanced at elevated temperatures.

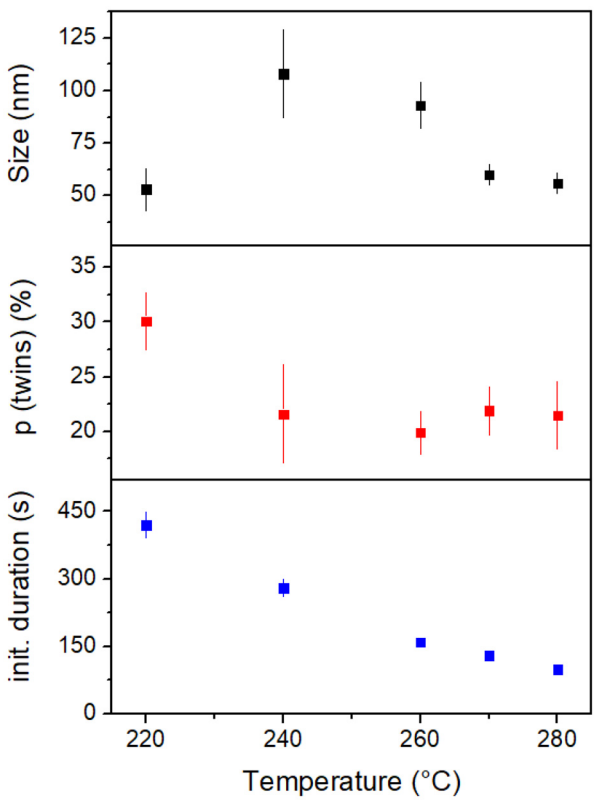

Fig. 5 Plots showing the temperature dependency of the nanoparticle edge lengths (top), the percentage of (multiply) twinned nanoparticles (p = percentage of MT crystals in relation to the total amount of Ag nanoparticles) (middle), and the duration of the color change of the initial reaction (bottom).

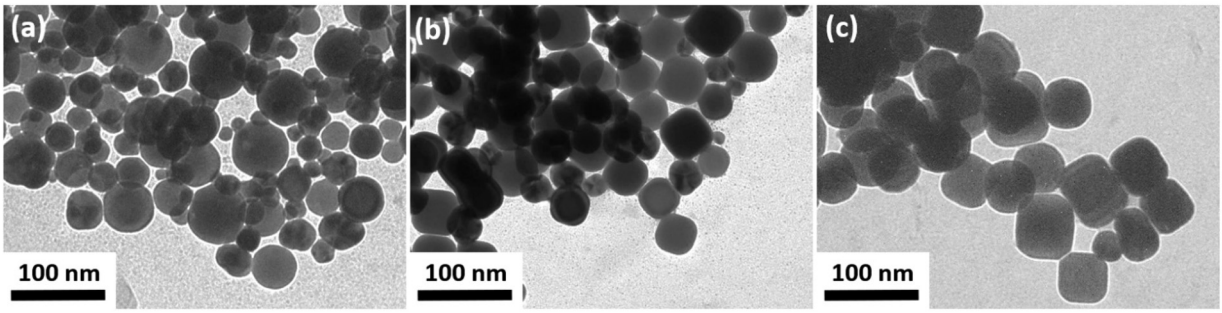

Fig. 6 TEM images of the Ag nanoparticles resulting from (a) a synthesis with Ag acetate as precursor instead of $AgNO_3$, (b) the standard synthesis, and (c) a synthesis with additional NH_4NO_3.

However, it appears that the reaction does not follow the expected course at a temperature of 220 °C (Fig. S6(a), ESI†). Other than at higher temperatures, the nanoparticles were irregularly shaped, and about 30% AgCl was still found in the sample. The sample consists of some high-quality nanocubes next to nanorods, spherical nanoparticles, and even some other structures. While the other samples seem to yield smaller particle sizes with increasing temperature and have about the same percentage of MT nanoparticles, the nanoparticles of the sample at 220 °C reaction temperature are the smallest ones, and significantly more MT nanoparticles are present. Consequently, it is assumed that a temperature of at least 240 °C is required for the educts to undergo the desired reaction.

The nanocubes obtained at 240 °C (see SEM image in Fig. S6(b), ESI†) have an edge length slightly larger than 100 nm and a polydispersity of around 20%. This result is comparable to the results at 260 °C with a higher chloride content. This trend continues for the reactions at 270 °C and 280 °C (Fig. S6(d) and (e), ESI†). The results resemble the results at 260 °C with a lower chloride content, *i.e.*, the higher the temperature, the smaller the nanoparticles, and the polydispersity is around 10%. This can be explained by a reduction rate that is more elevated than the oxidation rate. The question remains whether the oxidation rate is not as much elevated as the reduction rate or whether there is another rate-limiting factor.

The most important finding is that the percentage of MT nanoparticles does not change between 240–280 °C. This indicates that the oxidation of the MT nanoparticles is not affected by the temperature in this range. Rather, it is limited by the amount of chloride, which is strongly connected to the oxidation process.

Concluding that the reduction rate is increased with an elevated temperature and the oxidation rate is increased with a higher amount of chloride, another synthesis was performed at 290 °C with a chloride content of 0.55 mmol (instead of 0.525 mmol) (Fig. S6(f), ESI†). The resulting nanocubes had an edge length of 57 ± 4 nm, and the percentage of MT nanoparticles was reduced by almost half compared to the synthesis with a chloride content of 0.525 mmol. It should be noted that

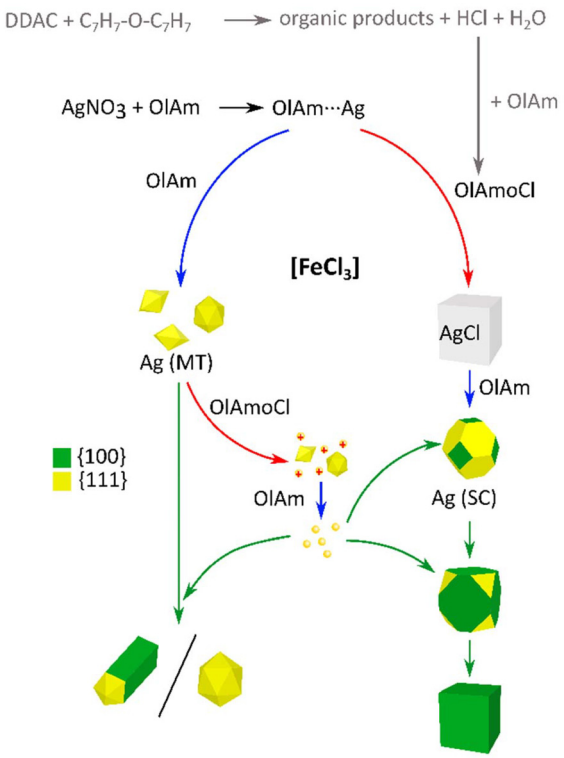

Scheme 1 Schematic representation of the mechanisms and influences leading from the precursors to the final products. The Ag precursor is formed from $AgNO_3$ and oleylamine (OlAm) and injected into the 260 °C hot oleylammonium chloride precursor (OlAmoCl) solution. The OlAmoCl is previously formed *in situ* by the reaction of dimethyldistearylammonium chloride (DDAC) with dibenzyl ether and OlAm. Alternatively, OlAmoCl can be prepared separately and added directly to the reaction mixture. During the thermal decomposition of the Ag-OlAm precursor, Ag^+ is either reduced and forms multiply twinned (MT) nanoparticles or forms AgCl with the aid of OlAmoCl. While the AgCl is reduced to single crystalline (SC) Ag nanoparticles, the MT nanoparticles are oxidized. The SC nanoparticles grow into nanocubes, and the remaining MT nanoparticles grow larger or transform into nanorods due to the attachment of Ag monomers from the reduced AgCl. The blue arrows indicate reduction, the red arrows oxidation, and the green arrows a coalescence process. $[FeCl_3]$ denotes the catalyst involved in the formation process.

the solvents OlAm and DBE had been in use for several weeks to months, during which time they may have undergone degradation.[61,62] With fresh solvents used, the amount of MT nanoparticles could be reduced by another ~50%.

Additional experiments demonstrated that at a reaction temperature of 290 °C, high-quality nanocubes can be obtained within a size range of ~50–100 nm. If the edge length is below 50 nm, the nanocubes become strongly truncated; if the edge length is above 100 nm, the polydispersity increases drastically. Furthermore, the reaction time can be reduced by 20 min to 40 min. Consequently, at a higher reaction temperature, a higher chloride content can be used to obtain the same nanocube sizes, and additionally, the amount of MT nanoparticles can be reduced.

Detailed growth mechanism

Based on the above-discussed results, the original growth mechanism proposed by Peng and Sun was extended.[47] The suggested modified mechanism is displayed in Scheme 1.

The chloride precursor was initially generated *in situ* from DDAC and OlAm. However, it could be shown that both compounds undergo a reaction and form OlAmoCl as the final chloride source in the reaction. Since OlAmoCl can be pre-synthesized, the synthesis becomes more controlled when it is used directly. The reaction steps displayed in gray in Scheme 1 are, therefore, no longer included in the optimized protocol.

After injection of the Ag-OlAm precursor into the hot reaction mixture, the Ag^+ ions are either reduced by OlAm and form MT Ag nanoparticles or form AgCl when they react with the Cl precursor. The probability of the two possible pathways depends on the chloride content in the reaction solution. If the MT nanoparticles are still small, they can be dissolved again and be reduced into Ag monomers. Simultaneously, SC Ag nanoparticles are formed from AgCl. The SC nanoparticles, as well as the remaining MT nanoparticles, grow larger due to the Ag monomers, which result from the reduction of the dissolved silver. Important for the growth of the nanoparticles into nanocubes (or nanorods) is the stabilization of the {100} facets, which happens because of the chloride species present (OlAmoCl).

Furthermore, $FeCl_3$ is identified as a crucial catalyst in the reaction mechanism. However, the exact influence of this catalyst requires further investigation.

Conclusions

This study demonstrated the importance of a detailed knowledge of the synthesis parameters in nanocrystal preparation. We designed a synthesis yielding high-quality nanocubes in a non-polar solvent mixture with a high reproducibility and a reaction time below 1 h. Iron ions proved to be crucial for the success of the synthesis due to their catalytic function in the reaction. Without the iron ions, no nanocubes could be obtained after 1 h of reaction time, and the sample consisted mainly of multiply twinned nanoparticles and still some AgCl. However, the exact influences of the Fe^{2+}/Fe^{3+} ions appear to be complex and requires further investigation. The Cl : Ag ratio also a significant factor, as the results are strongly influenced by it. If the ratio is too small, no nanocubes are formed. If the ratio is too large, the nanocubes are highly polydisperse, and AgCl is present in the final sample. The chloride source originally used was not stable, and the ratio could easily vary. We found that the final chloride species in the reaction was oleylammonium chloride. When it is directly added to the reaction as the chloride precursor, the Cl : Ag ratio can be precisely controlled, and nanocubes with edge lengths in the range of 40–100 nm can be obtained. The chloride concentration also seems to affect the oxidative etching process and in combination with a higher reaction temperature, a higher Cl : Ag ratio significantly reduces the percentage of multiply twinned nanoparticles. Oxygen, however, does not promote the oxidative etching in this reaction, although this has been reported for other synthesis of silver nanocubes. The nanocubes obtained by the presented protocol exhibit a number of advantageous characteristics, including a short production time, sharp edges, low polydispersity, high reproducibility, widely adjustable edge lengths, and, thus, adjustable optical properties. These properties make the nanocubes excellent candidates for applications in catalysis, photonics, sensor technology, and other fields. The present work demonstrates that a thorough analysis and optimization of the reaction parameters in nanoparticle syntheses allows the transformation of an initially rather random synthesis into a precisely defined and widely adjustable preparation process. We expect that this methodological approach and our results can be transferred to other synthesis processes of anisotropic nanocrystals, especially in non-polar solvents.

Author contributions

M. Joschko: design and development of the synthesis, characterization of the samples, and preparation of the original draft. M. Schattmann: design and development of the synthesis. D. Grollmusz: optimization of the synthesis. C. Graf: acquisition of funding, supervision, project management, review, and editing of the manuscript.

Data availability

The data supporting this article have been included as part of the ESI.†

Additional TEM and SEM images are available in TIFF form as well as X-ray diffractograms as ASCII file from the authors upon request.

Conflicts of interest

There are no conflicts to declare.

Acknowledgements

We thank Julia Mausz of EDAX AMETEK for her help in correcting the EDX results with standards.

This work was financially supported by a fellowship of the platform for PhD students of Technische Universität Darmstadt and Darmstadt University of Applied Sciences, by the Graduate School of the Darmstadt University of Applied Sciences, and by a mid-level faculty position at Darmstadt University of Applied Sciences.

References

1 T. W. Purcell and J. J. Peters, Sources of Silver in the Environment, *Environ. Toxicol. Chem.*, 1998, **17**, 539–546.
2 J. Natsuki, A Review of Silver Nanoparticles: Synthesis Methods, Properties and Applications, *Int. J. Sport Nutr. Exercise Metab.*, 2015, **4**, 325.
3 A. H. Alshehri, M. Jakubowska, A. Młożniak, M. Horaczek, D. Rudka, C. Free and J. D. Carey, Enhanced Electrical Conductivity of Silver Nanoparticles for High Frequency Electronic applications, *ACS Appl. Mater. Interfaces*, 2012, **4**, 7007–7010.
4 A. Bouafia, S. E. Laouini, A. S. A. Ahmed, A. V. Soldatov, H. Algarni, K. F. Chong and G. A. M. Ali, The Recent Progress on Silver Nanoparticles: Synthesis and Electronic Applications, *Nanomaterials*, 2021, **11**, 2318, DOI: **10.3390/nano11092318**.
5 L. Mo, Z. Guo, L. Yang, Q. Zhang, Y. Fang, Z. Xin, Z. Chen, K. Hu, L. Han and L. Li, Silver Nanoparticles Based Ink with Moderate Sintering in Flexible and Printed Electronics, *Int. J. Mol. Sci.*, 2019, **20**, 2124, DOI: **10.3390/ijms20092124**.
6 K. Phoonsawat, N. Ratnarathorn, C. S. Henry and W. Dungchai, A Distance-Based Paper Sensor for the Determination of Chloride Ions Using Silver Nanoparticles, *Analyst*, 2018, **143**, 3867–3873.
7 P. Prosposito, L. Burratti and I. Venditti, Silver Nanoparticles as Colorimetric Sensors for Water Pollutants, *Chemosensors*, 2020, **8**, 26.
8 C. J. Kirubaharan, D. Kalpana, Y. S. Lee, A. R. Kim, D. J. Yoo, K. S. Nahm and G. G. Kumar, Biomediated Silver Nanoparticles for the Highly Selective Copper(II) Ion Sensor Applications, *Ind. Eng. Chem. Res.*, 2012, **51**, 7441–7446.
9 N. Durán, M. Durán, M. B. de Jesus, A. B. Seabra, W. J. Fávaro and G. Nakazato, Silver Nanoparticles: A New View on Mechanistic Aspects on Antimicrobial Activity, *Nanomedicine*, 2016, **12**, 789–799.
10 I.-S. Hwang, J. H. Hwang, H. Choi, K.-J. Kim and D. G. Lee, Synergistic Effects between Silver Nanoparticles and Antibiotics and the Mechanisms Involved, *J. Med. Microbiol.*, 2012, **61**, 1719–1726.
11 M. Rai, A. Yadav and A. Gade, Silver Nanoparticles as a New Generation of Antimicrobials, *Biotechnol. Adv.*, 2009, **27**, 76–83.
12 K. Awazu, M. Fujimaki, C. Rockstuhl, J. Tominaga, H. Murakami, Y. Ohki, N. Yoshida and T. Watanabe, A Plasmonic Photocatalyst Consisting of Silver Nanoparticles Embedded in Titanium dioxide, *J. Am. Chem. Soc.*, 2008, **130**, 1676–1680.
13 G. Merga, R. Wilson, G. Lynn, B. H. Milosavljevic and D. Meisel, Redox Catalysis on "Naked" Silver Nanoparticles, *J. Phys. Chem. C*, 2007, **111**, 12220–12226.
14 N. Pradhan, A. Pal and T. Pal, Silver Nanoparticle Catalyzed Reduction of Aromatic Nitro Compounds, *Colloids Surf., A*, 2002, **196**, 247–257.
15 M. Fan and A. G. Brolo, Silver Nanoparticles Self Assembly as SERS Substrates with Near Single Molecule Detection Limit, *Phys. Chem. Chem. Phys.*, 2009, **11**, 7381–7389.
16 R. X. He, R. Liang, P. Peng and Y. N. Zhou, Effect of the Size of Silver Nanoparticles on SERS Signal Enhancement, *J. Nanopart. Res.*, 2017, **19**, 1–10.
17 Y. Yang, S. Matsubara, L. Xiong, T. Hayakawa and M. Nogami, Solvothermal Synthesis of Multiple Shapes of Silver Nanoparticles and Their SERS Properties, *J. Phys. Chem. C*, 2007, **111**, 9095–9104.
18 C. Wang, B. Liu and X. Dou, Silver Nanotriangles-Loaded Filter Paper for Ultrasensitive SERS Detection Application Benefited by Interspacing of Sharp Edges, *Sens. Actuators, B*, 2016, **231**, 357–364.
19 Q. Wang, X. Cui, W. Guan, L. Zhang, X. Fan, Z. Shi and W. Zheng, Shape-Dependent Catalytic Activity of Oxygen Reduction Reaction (ORR) on Silver Nanodecahedra and Nanocubes, *J. Power Sources*, 2014, **269**, 152–157.
20 L. Du, Q. Xu, M. Huang, L. Xian and J.-X. Feng, Synthesis of Small Silver Nanoparticles under Light Radiation by Fungus Penicillium oxalicum and its application for the catalytic reduction of methylene blue, *Mater. Chem. Phys.*, 2015, **160**, 40–47.
21 R. Xu, D. Wang, J. Zhang and Y. Li, Shape-Dependent Catalytic Activity of Silver Nanoparticles for the Oxidation of Styrene, *Chem. – Asian J.*, 2006, **1**, 888–893.
22 S. S. Sangaru, H. Zhu, D. C. Rosenfeld, A. K. Samal, D. Anjum and J.-M. Basset, Surface Composition of Silver Nanocubes and Their Influence on Morphological Stabilization and Catalytic Performance in Ethylene Epoxidation, *ACS Appl. Mater. Interfaces*, 2015, **7**, 28576–28584.
23 L. D. Marks, Experimental Studies of Small Particle Structures, *Rep. Prog. Phys.*, 1994, **57**, 603–649.
24 B. Wiley, Y. Sun, B. Mayers and Y. Xia, Shape-Controlled Synthesis of Metal Nanostructures: the Case of Silver, *Chemistry*, 2005, **11**, 454–463.
25 Y. Sun and Y. Xia, Shape-Controlled Synthesis of Gold and Silver Nanoparticles, *Science*, 2002, **298**, 2176–2179.
26 B. Wiley, T. Herricks, Y. Sun and Y. Xia, Polyol Synthesis of Silver Nanoparticles: Use of Chloride and Oxygen to Promote the Formation of Single-Crystal, Truncated Cubes and Tetrahedrons, *Nano Lett.*, 2004, **4**, 1733–1739.

27 S. H. Im, Y. T. Lee, B. Wiley and Y. Xia, Large-Scale Synthesis of Silver Nanocubes: the Role of HCl in Promoting Cube Perfection and Monodispersity, *Angew. Chem., Int. Ed.*, 2005, **44**, 2154–2157.
28 Y. T. Lee, S. H. Im, B. Wiley and Y. Xia, Quick Formation of Single-Crystal Nanocubes of Silver Through Dual Functions of Hydrogen Gas in Polyol Synthesis, *Chem. Phys. Lett.*, 2005, **411**, 479–483.
29 A. R. Siekkinen, J. M. McLellan, J. Chen and Y. Xia, Rapid Synthesis of Small Silver Nanocubes by Mediating Polyol Reduction with a Trace Amount of Sodium Sulfide or Sodium Hydrosulfide, *Chem. Phys. Lett.*, 2006, **432**, 491–496.
30 Q. Zhang, C. Cobley, L. Au, M. McKiernan, A. Schwartz, L.-P. Wen, J. Chen and Y. Xia, Production of Ag Nanocubes on a Scale of 0.1 g per Batch by Protecting the NaHS-Mediated Polyol Synthesis with Argon, *ACS Appl. Mater. Interfaces*, 2009, **1**, 2044–2048.
31 Y. Wang, Y. Zheng, C. Z. Huang and Y. Xia, Synthesis of Ag Nanocubes 18-32 nm in Edge Length: the Effects of Polyol on Reduction kinetics, size control, and reproducibility, *J. Am. Chem. Soc.*, 2013, **135**, 1941–1951.
32 Q. Zhang, W. Li, L.-P. Wen, J. Chen and Y. Xia, Facile Synthesis of Ag Nanocubes of 30 to 70 nm in Edge Length with CF(3)COOAg As a Precursor, *Chemistry*, 2010, **16**, 10234–10239.
33 A. Ruditskiy and Y. Xia, Toward the Synthesis of Sub-15 nm Ag Nanocubes with Sharp Corners and Edges: The Roles of Heterogeneous Nucleation and Surface Capping, *J. Am. Chem. Soc.*, 2016, **138**, 3161–3167.
34 S. Zhou, J. Li, K. D. Gilroy, J. Tao, C. Zhu, X. Yang, X. Sun and Y. Xia, Facile Synthesis of Silver Nanocubes with Sharp Corners and Edges in an Aqueous Solution, *ACS Nano*, 2016, **10**, 9861–9870.
35 S. Zhou, D. S. Mesina, M. A. Organt, T.-H. Yang, X. Yang, D. Huo, M. Zhao and Y. Xia, Site-Selective Growth of Ag Nanocubes for Sharpening Their Corners and Edges, Followed by Elongation into Nanobars Through Symmetry Reduction, *J. Mater. Chem. C*, 2018, **6**, 1384–1392.
36 D. Yu and V. W.-W. Yam, Controlled Synthesis of Monodisperse Silver Nanocubes in Water, *J. Am. Chem. Soc.*, 2004, **126**, 13200–13201.
37 Z.-W. Lin, Y.-C. Tsao, M.-Y. Yang and M. H. Huang, Seed-Mediated Growth of Silver Nanocubes in Aqueous Solution with Tunable Size and Their Conversion to Au Nanocages with Efficient Photothermal Property, *Chemistry*, 2016, **22**, 2326–2332.
38 L. Polavarapu and L. M. Liz-Marzán, Towards Low-Cost Flexible Substrates for Nanoplasmonic Sensing, *Phys. Chem. Chem. Phys.*, 2013, **15**, 5288–5300.
39 A. Sánchez-Iglesias, M. Grzelczak, J. Pérez-Juste and L. M. Liz-Marzán, Binary Self-Assembly of Gold Nanowires with Nanospheres and Nanorods, *Angew. Chem., Int. Ed.*, 2010, **49**, 9985–9989.
40 M. Chen, Y.-G. Feng, X. Wang, T.-C. Li, J.-Y. Zhang and D.-J. Qian, Silver nanoparticles capped by oleylamine: formation, growth, and self-organization, *Langmuir*, 2007, **23**, 5296–5304.
41 L. Lin, M. Chen, H. Qin and X. Peng, Ag Nanocrystals with Nearly Ideal Optical Quality: Synthesis, Growth Mechanism, and Characterizations, *J. Am. Chem. Soc.*, 2018, **140**, 17734–17742.
42 S. Mourdikoudis, M. Menelaou, N. Fiuza-Maneiro, G. Zheng, S. Wei, J. Pérez-Juste, L. Polavarapu and Z. Sofer, Oleic acid/oleylamine ligand pair: a versatile combination in the synthesis of colloidal nanoparticles, *Nanoscale Horiz.*, 2022, **7**, 941–1015.
43 J. Pan, W. Wang, M. Ji, X. Xing and Z. Lu, Robust Synthesis of Silver Nanocubes in Oil Phase, *Cryst. Growth*, 2023, **23**, 2203–2208.
44 L. Polavarapu and L. M. Liz-Marzán, Growth and Galvanic Replacement of Silver Nanocubes in Organic Media, *Nanoscale*, 2013, **5**, 4355–4361.
45 Y. Ma, W. Li, J. Zeng, M. McKiernan, Z. Xie and Y. Xia, Synthesis of Small Silver Nanocubes in a Hydrophobic Solvent by Introducing Oxidative Etching with Fe(iii) Species, *J. Mater. Chem.*, 2010, **20**, 3586.
46 S. Peng, J. S. Okasinski, J. D. Almer, Y. Ren, L. Wang, W. Yang and Y. Sun, Real-Time Probing of the Synthesis of Colloidal Silver Nanocubes with Time-Resolved High-Energy Synchrotron X-ray Diffraction, *J. Phys. Chem. C*, 2012, **116**, 11842–11847.
47 S. Peng and Y. Sun, Synthesis of Silver Nanocubes in a Hydrophobic Binary Organic Solvent, *Chem. Mater.*, 2010, **22**, 6272–6279.
48 A. Dutta, R. K. Behera, S. K. Dutta, S. D. Adhikari and N. Pradhan, Annealing CsPbX3 (X = Cl and Br) Perovskite Nanocrystals at High Reaction Temperatures: Phase Change and Its Prevention, *J. Phys. Chem. Lett.*, 2018, **9**, 6599–6604.
49 Coblentz Society Inc., in *NIST Chemistry WebBook*, ed. P. J. Linstrom and W. G. Mallard, National Institute of Standards and Technology, Gaithersburg MD, 2025, p. 20899, DOI: DOI: **10.18434/T4D303**.
50 D. Häfner, *Arbeitsbuch Qualitative Anorganische Analyse. Für Pharmazie- und Chemiestudenten*, Govi-Verl., Eschborn, 2nd edn, 2003.
51 T. Frederick and A. Bell, Cleavage of Dibenzyl Ether in the Presence of Zinc Halides, *J. Catal.*, 1984, **87**, 226–237.
52 Z. Fan, L. Zhang, S. Liu, L. Luan, G. Li and D. Sun, Mechanism of High Temperature Induced Destabilization of Nonpolar Organoclay suspension, *J. Colloid Interface Sci.*, 2019, **555**, 53–63.
53 E. S. A. Nouh, E. A. Baquero, L.-M. Lacroix, F. Delpech, R. Poteau and G. Viau, Surface-Engineering of Ultrathin Gold Nanowires: Tailored Self-Assembly and Enhanced Stability, *Langmuir*, 2017, **33**, 5456–5463.
54 V. Grigel, L. K. Sagar, K. de Nolf, Q. Zhao, A. Vantomme, J. de Roo, I. Infante and Z. Hens, The Surface Chemistry of Colloidal HgSe Nanocrystals, toward Stoichiometric Quantum Dots by Design, *Chem. Mater.*, 2018, **30**, 7637–7647.

55 S. Chen, J. L. Carey, D. R. Whitcomb, P. Bühlmann and R. L. Penn, Elucidating the Role of AgCl in the Nucleation and Growth of Silver Nanoparticles in Ethylene Glycol, *Cryst. Growth Des.*, 2018, **18**, 324–330.
56 W. M. Schuette and W. E. Buhro, Silver chloride as a heterogeneous nucleant for the growth of silver nanowires, *ACS Nano*, 2013, **7**, 3844–3853.
57 C. Goessens, D. Schryvers, J. van Landuyt and R. de Keyzer, In situ HREM study of electron irradiation effects in AgCl microcrystals, *Ultramicroscopy*, 1992, **40**, 151–162.
58 C. Ni, P. A. Hassan and E. W. Kaler, Structural Characteristics and Growth of Pentagonal Silver Nanorods Prepared by a Surfactant Method, *Langmuir*, 2005, **21**, 3334–3337.
59 M. Calcabrini, D. van den Eynden, S. S. Ribot, R. Pokratath, J. Llorca, J. de Roo and M. Ibáñez, Ligand Conversion in Nanocrystal Synthesis: The Oxidation of Alkylamines to Fatty Acids by Nitrate, *JACS Au*, 2021, **1**, 1898–1903.
60 D. Sridaeng, A. Limsirinawa, P. Sirojpornphasut, S. Chawiwannakorn and N. Chantarasiri, Metal acetylacetonate–amine and metal nitrate–amine complexes as low–emission catalysts for rigid polyurethane foam preparation, *J. Appl. Polym. Sci.*, 2015, **132**, 42332, DOI: **10.1002/app.42332**.
61 D. Baranov, M. J. Lynch, A. C. Curtis, A. R. Carollo, C. R. Douglass, A. M. Mateo-Tejada and D. M. Jonas, Purification of Oleylamine for Materials Synthesis and Spectroscopic Diagnostics for trans Isomers, *Chem. Mater.*, 2019, **31**, 1223–1230.
62 F. G. Eichel and D. F. Othmer, Benzaldehyde by Autoxidation by Dibenzyl Ether, *Ind. Eng. Chem.*, 1949, **41**, 2623–2626.